Optical initialization of a single spin-valley in charged WSe₂ quantum dots

Xin Lu^{1,4}, Xiaotong Chen^{1,4}, Sudipta Dubey^{1,4}, Qiang Yao¹, Weijie Li¹, Xingzhi Wang², Qihua Xiong^{2,3} and Aiit Srivastava¹

Control and manipulation of single charges and their internal degrees of freedom, such as spin, may enable applications in quantum information technology, spintronics and quantum sensing^{1,2}. Recently, atomically thin semiconductors with a direct bandgap such as group VI-B transition-metal dichalcogenide monolayers have emerged as a platform for valleytronics—the study of the valley degree of freedom of charge carriers to store and control information. They offer optical, magnetic and electrical control of the valley index, which, with the spin, is locked into a robust spin-valley index^{3,4}. However, because recombination lifetimes of photogenerated excitations in transition-metal dichalcogenides are of the order of a few picoseconds, optically generated valley excitons possess similar lifetimes. On the other hand, the valley polarization of free holes has a lifetime of microseconds⁵⁻⁹. Whereas progress has been made in optical control of the valley index in ensembles of charge carriers¹⁰⁻¹², valley control of individual charges, which is crucial for valleytronics, remains unexplored. Here we provide unambiguous evidence for localized holes with a net spin in optically active WSe, quantum dots13-17 and we initialize their spin-valley state with the helicity of the excitation laser under small magnetic fields. Under such conditions, we estimate a lower bound of the valley lifetime of a single charge in a quantum dot from the recombination time to be of the order of nanoseconds. Remarkably, neutral quantum dots do not exhibit such spin-valley initialization, which illustrates the role of the excess charge in prolonging the valley lifetime. Our work extends the field of two-dimensional valleytronics to the level of single spin-valleys, with implications for quantum information and sensing applications.

Quantum dots (QDs) in transition-metal dichalcogenides (TMDs) such as WSe₂ are believed to be excitons trapped in shallow potential wells arising from either defects or localized strain on the monolayer flake^{18–20}. Furthermore, they seem to inherit the valley physics of the two-dimensional exciton, as suggested by their extreme anisotropic response with respect to an in-plane versus out-of-plane magnetic field, B^{21} . Given that valley mixing seems to be absent in these QDs, the length scale of confinement must be larger than the Bohr radius of excitons and trions (about 1-2 nm)²². Thus, we can safely assume that the single-particle band structure that is used to understand the two-dimensional exciton should be applicable to the neutral and singly charged QDs as well. Figure 1a,b shows the contrast between valley configurations of the single-particle states, which constitute a negatively charged QD (X_d^-) and a

positively charged QD (X_d^+) , respectively. X_d^- has two inequivalent configurations where the excess electron is in the same or opposite valley as the electron-hole pair. For a fixed spin-valley of the excess electron, the same-valley and opposite-valley X_d^- configurations are mixed by the electron-hole exchange of the exciton (J_{eb}) and also split by the electron-hole exchange between the excess electron and the hole $(J'_{eh})^{23,24}$. As a result, the valleys of the exciton in X_d^- are mixed, even though the spins of the excess electron are not, leading to a loss of helicity control of the electron spin-valley (see Supplementary Information section 1). On the other hand, the excess hole in X_d^+ can only be in the opposite-valley configuration, owing to the large spin-orbit coupling in the valence band, in which case the electron-hole exchange interaction between the excess hole and the electron (J'_{eh}) is quenched. Thus, the valley index of the exciton in X_d^+ is perfectly anti-correlated with that of the excess hole. As a result, the helicity of X_d^+ emission that depends on the valley index of the recombining electron-hole pair can be used to read out the spin-valley of the excess hole. Moreover, J_{eh} should also be strongly suppressed upon localization into a QD owing to Pauli blockade (Fig. 1b). The quenching of electron-hole exchange in X_d^+ should prevent valley mixing and lead to helicity-based initialization of single-hole spin with longer spin-valley lifetimes, which is desirable for spin-valleytronics.

Figure 1c shows a charge-tuneable, monolayer WSe₂ field effect transistor device, which we use to obtain charged QDs (see Methods). By electrostatic doping, we inject free holes or electrons in the monolayer sample, which then contributes to a current under an applied source–drain bias. Figure 1d shows that the sample has a higher propensity for hole-doping than electron-doping, as can be seen from the dominant hole current at negative gate voltage $V_{\rm g}$. These free carriers can then be trapped in QDs, giving rise to localized charges in QDs. In our experiments, we operate close to the hole-doped regime of $V_{\rm g}$ where only free holes are expected to be present in the monolayer. Our device should be contrasted with a tunnel-coupling device where charge carriers tunnel in and out of the QD from nearby leads resulting in charge-controlled emission²⁵.

We perform $V_{\rm g}$ -dependent photoluminescence spectroscopy on the monolayer WSe₂ field effect transistor device at low incident powers (see Methods). Figure 2a,b (or Fig. 2c,d) shows photoluminescence intensity maps (or cross-sectional photoluminescence spectra) of a set of peaks appearing at a certain negative $V_{\rm g}$ when the sample is expected to be lightly hole-doped. For example, at $V_{\rm g} \approx -10$ V, a single peak labelled S1 and a doublet labelled D1 appear simultaneously and spectrally wander in an identical manner, as

¹Department of Physics, Emory University, Atlanta, GA, USA. ²Division of Physics and Applied Physics, School of Physical and Mathematical Sciences, Nanyang Technological University, Singapore, Singapore. ³NOVITAS, Nanoelectronics Centre of Excellence, School of Electrical and Electronic Engineering, Nanyang Technological University, Singapore, Singapore. ⁴These authors contributed equally: Xin Lu, Xiaotong Chen, Sudipta Dubey.
*e-mail: xin.lu2@emory.edu; ajit.srivastava@emory.edu

LETTERS

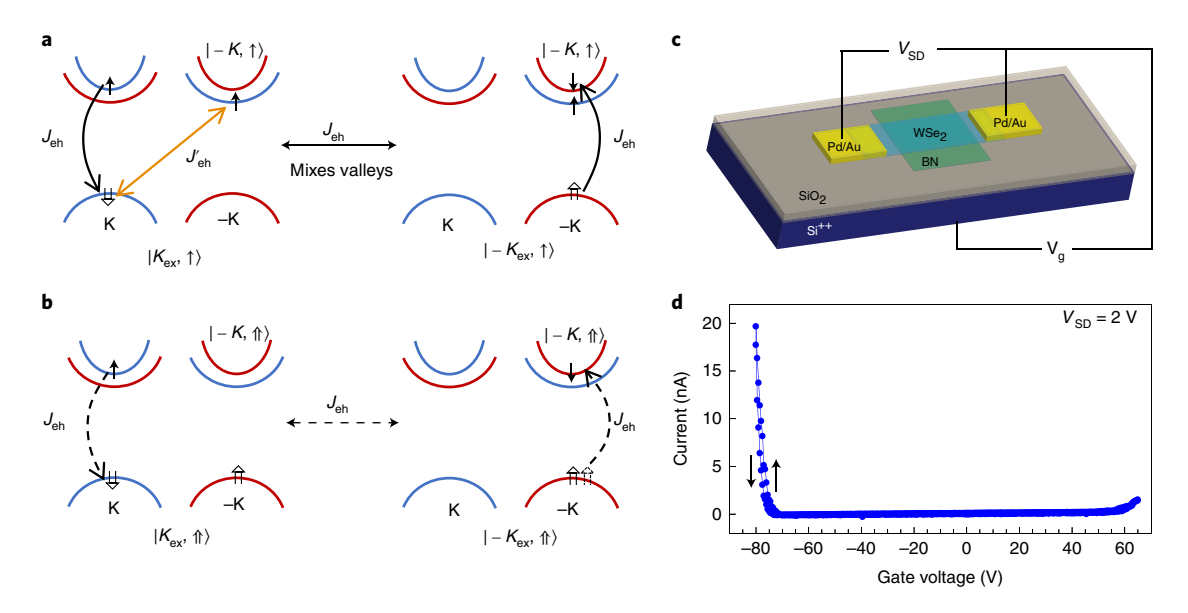


Fig. 1 | Singly charged QDs and charge control in a monolayer WSe₂ field effect transistor. **a**, Schematic illustration of the single-particle states comprising a negatively charged QD (X_d^-) with an exciton in the K valley and the excess electron in the -K valley (left panel). Electron and hole spins are depicted with single- and double-line arrows, respectively. Electron spin-up (or spin-down) bands appear in blue (or red). The long-range exchange interaction J_{eh} (electron and hole in the same valley) mixes the opposite-valley and same-valley X_d^- (right panel) configurations. Consequently, the valleys of the exciton in X_d^- are mixed, while the spins of the excess electron are not. The short-range exchange (J'_{eh}) splits the same-valley and opposite-valley configurations. **b**, Schematic illustration of the single-particle states comprising a positively charged QD (X_d^+) with an exciton in the K valley and the excess hole in the -K valley (left panel). J'_{eh} is quenched owing to holes forming a singlet and J_{eh} is expected to be strongly suppressed because of Pauli blocking when charges are localized in a QD (right panel). $|-K,\uparrow\rangle$ (or $|-K,\uparrow\rangle$) shows the spin-valley state of the excess electron (or hole). $|K_{ex},\uparrow\rangle$ (or $|-K_{ex},\uparrow\rangle$) shows the valley of the recombination exciton K_{ex} (or $-K_{ex}$) and the state of the excess hole. **c**, **d**, Monolayer WSe₂ field effect transistor device. **c**, Schematic of the field effect transistor device. **d**, The field effect transistor current I_{SD} versus gate voltage measured with a source-drain voltage of $V_{SD} = 2$ V. The arrows indicate forward and backward sweeps, respectively.

highlighted by the solid circles (Fig. 2a). Thus we can conclude that the peaks S1 and D1 arise from the same QD. Likewise, at another location on the sample, the S2-D2 group (see Supplementary Fig. 1 for the S6-D6 group) also displays the same turn-on voltage and jittering pattern (Fig. 2b).

The energy splitting of the doublets is about 600 µeV, which is consistent with the fine structure splitting resulting from the anisotropic electron-hole exchange interaction reported in previous studies on optically active neutral QDs in TMDs^{13,14,16}. Thus we assign D-peaks to neutral QDs, X_d^0 . We notice that the energy spacing between S- and D-peaks is about 10 meV for all QDs, with S-peaks located at higher energy. Unlike neutral and evenly charged excitons where electron-hole exchange interaction causes a fine structure splitting, in a singly, positively charged QD the electron-hole exchange interaction is expected to vanish, as discussed earlier. Given that the sample is devoid of electrons in the range of V_g where S-peaks are observed, we assign S-peaks to X_d^+ . We contrast our findings with recently reported negatively charged QDs in WSe₂ where a fine structure splitting was seen, unlike in ref. ²⁶. We note that the X_d^+ state has a binding energy $(E_{X_d^0} - E_{X_d^+})$ of $-10 \,\mathrm{meV}$ with respect to X_d^0 , which could originate from the Coulomb repulsion between holes and details of electron and hole wave functions in the QD (see Supplementary Table 1). Indeed, negative binding energy of X_d^+ has been reported in InGaAs QDs as opposed to $X_d^$ and attributed to the different confining potentials for electrons and holes²⁷. Figure 2e shows that the excitation power-dependence of the S1-D1 group exhibits a similar power-law behaviour consistent with our assignments and rules out a positively charged biexciton as a possible origin of S-peaks (see also Supplementary Fig. 2).

The coexistence of neutral QDs, $X_{\rm d}^0$ and positively charged QDs, $X_{\rm d}^+$, at $V_{\rm g}$ <0 during integration times of the order of tens of

seconds indicates that the excess hole is trapped and released by X_0^0 on a much faster timescale, which also determines the relative intensity of S- and D-peaks. However, as shown in Fig. 2f–h, occasionally an anti-correlation is seen in the intensity of S- and D-peaks at longer timescales. This anti-correlation in the intensities of S1- and D1-peaks is consistent with the picture that the excess hole is captured (or released) by the QD during emission at the energy of S-peaks (or D-peaks) and also corroborates our claim that the peaks arise from the same QD (see also Supplementary Fig. 3).

Having established that we observe positively charged and neutral excitons from the same QD, we perform polarization-resolved B measurements in a Faraday configuration. Figure 3a-c shows that both S- and D-peaks display a Zeeman splitting in B (see also Supplementary Fig. 4). However, unlike D-peaks, S-peaks show a linear, 'X'-shaped splitting consistent with the behaviour of a singly charged QD with no fine structure splitting25. We extract the corresponding g-factors, which are plotted in Fig. 3d-g. The value of the g-factors (approximately 10) of D1 and D2 is consistent with previous studies of neutral QDs in WSe₂¹³⁻¹⁶. A larger g-factor (of approximately 13) is observed for S-peaks and is consistent with the trend that X^{\pm} (delocalized trions) have a larger g-factor than X^{0} (free excitons)²¹ (see Supplementary Table 2). This difference in *g*-factors arises from the Coulomb interactions between electron and holes in the charged exciton state, that is, the initial state of the optical recombination process.

We also note that the intensities of the red and blue split peaks of the S-peaks are comparable even at the highest applied *B*. This behaviour is qualitatively different from that of the neutral D-peaks under *B*, the majority of which show emission only from the lowenergy peak (see also Supplementary Figs. 14 and 15). As the relaxation time after non-resonant excitation is much shorter than the

LETTERS NATURE NANOTECHNOLOGY

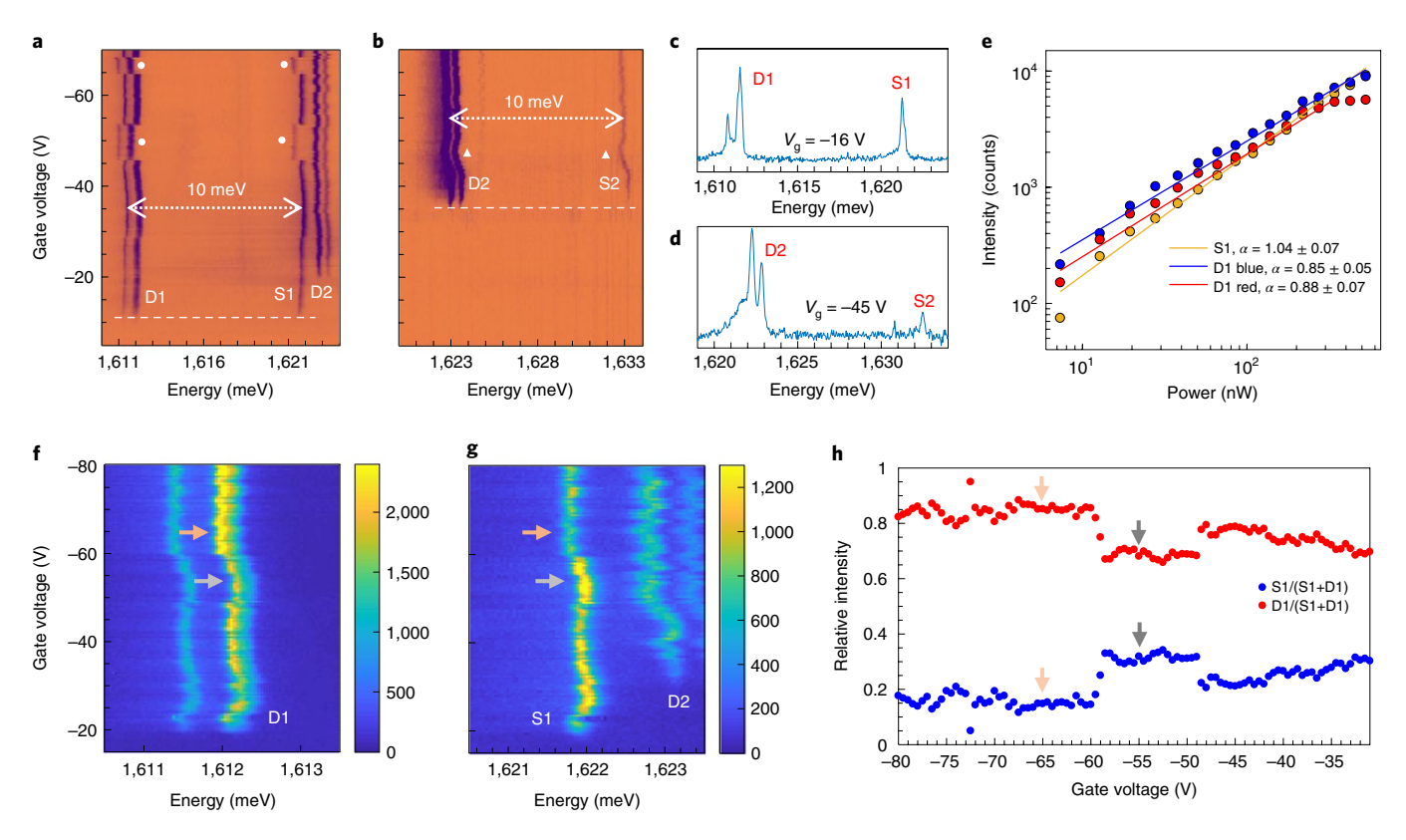


Fig. 2 | Charged and neutral QDs in monolayer WSe₂. a, b, Photoluminescence intensity maps as a function of gate voltage (V_g) from two different scans. S1 and D1, as well as S2 and D2, have correlated spectral jittering patterns (highlighted by solid symbols) and the same turn-on voltage (dashed line), respectively. As a result, they are assigned to the same QD groups. The energy spacing between the S- and D-peaks is about 10 meV for all QDs. **c, d,** Cross-sectional photoluminescence spectra at fixed V_g showing clear single- and double-peak features. **e,** Power dependence of the S1-D1 group. The lines fit the power law $I \propto P^\alpha$. The extracted values of α are similar for the S1 and D1 peaks. **f-h,** Anti-correlated intensity between S1 and D1. **f, g,** A V_g -dependent photoluminescence intensity map of the S1-D1 group. S1 is stronger (weaker) when the blue D1 peak is weaker (stronger), as indicated by grey (light orange) arrows. Colour bars indicate intensity (counts). **h,** Extracted relative intensity of S1 (blue dots) and D1 doublets (red dots). Laser excitation wavelengths, λ , for the S1-D1 and S2-D2 groups are 735 nm and 747 nm, respectively.

recombination time, in photoluminescence one expects emission mainly from the lowest-energy state, owing to thermalization. We therefore conclude that B-split states of X_d^+ before recombination (initial states) must have similar energies leading to similar emission intensities. This is qualitatively consistent with the single-particle picture of Fig. 1b where the excess hole resides in the opposite valley and hence shifts in the opposite direction from that of the hole of the recombining electron–hole pair 21,28 . As a result, the net energy difference in the B-split initial states of X_d^+ is reduced, resulting in similar emission intensities.

Next, we analyse the polarization of the S1 peak as a function of B. Figure 3h-i shows the DCP for a linearly polarized excitation laser where DCP is defined as $(I_{\sigma^+} - I_{\sigma^-}) / (I_{\sigma^+} + I_{\sigma^-})$, with I_{σ^+} (or I_{σ}^{-}) denoting the intensity of the σ^{+} (or σ^{-}) circularly polarized emission. The linearly polarized excitation laser is approximately 33 meV blue-detuned with respect to the emission at B = 0. At B = 0, we find that DCP is vanishingly small, implying that S1 is unpolarized (see Supplementary Fig. 6 for linear basis measurements). As X_d^+ is doubly degenerate at B=0 with energies of $|K_{ex}\rangle$ $\uparrow \rangle$ and $|-K_{ex}, \downarrow \rangle$ being equal, an unpolarized emission is indeed expected if the excitation laser is not exactly resonant with X_d^+ . As the *B* is increased, the DCP increases in magnitude, implying that the split peaks become circularly polarized. The σ^+ (or σ^-) emission is at lower (or higher) energy at positive B, and shifts to higher (or lower) energy at negative *B*. This can be understood by the fact that in finite B, the degeneracy of $K_{\rm ex}$ and $-K_{\rm ex}$ is lifted owing to the valley Zeeman effect^{21,22,28-30}. As the emission from X_d^+ takes place with $K_{\rm ex}$ (or $-K_{\rm ex}$) recombining to give σ^+ (or σ^-) polarized photon, we expect circularly polarized emission in finite B. This DCP results from the applied B, which breaks time-reversal symmetry, and not from optical excitation, which is kept linearly polarized. We note that S1 gets a sizeable circular component even at a small B ($B \approx 0.3$ T) as there is no exchange interaction to overcome, unlike in the case of X_d^0 . The applied B does not influence the circular polarization of S1 once DCP is saturated (see Supplementary Figs. 7 and 8 for S2).

As shown above, the degeneracy of X_d^+ is lifted in non-zero B, which allows us to spectrally distinguish between the spin-valley states $(|-K, \uparrow \rangle)$ or $|K, \downarrow \rangle$ of the excess hole. As the valley index of the exciton in X_d^+ is not mixed, we expect that controlling the helicity of the excitation laser should result in selective initialization of the spin-valley of the excess hole in X_d^+ , which is anti-correlated with the helicity of the recombining electron-hole pair. Figure 4a-c shows the *B* dependence of S2 (low energy peak) for σ^+ , σ^- and linear (π) excitation. Indeed, by using σ^+ excitation, we observe only the red peak of S2 at positive B, which corresponds to recombination of K_{ex} with σ^+ polarization (co-polarized with excitation) while the emission from $-K_{\rm ex}$ with σ^+ polarization (cross-polarized with excitation) completely disappears. The opposite case is observed with σ^- excitation, while for linear excitation both branches are observed (see also Supplementary Fig. 16). As the valley index of the excess hole is opposite to that of the recombining exciton, we

LETTERS

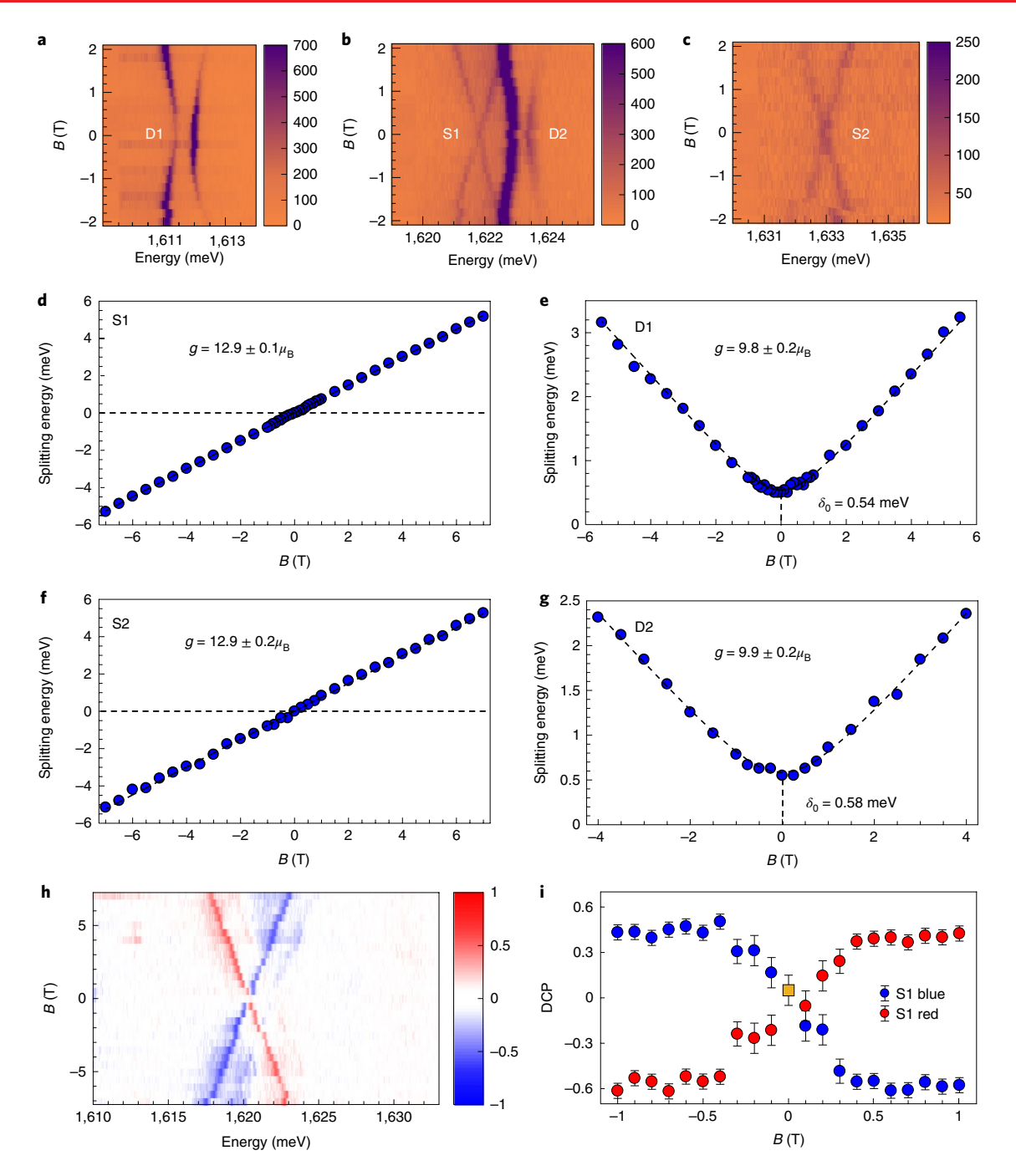


Fig. 3 | Zeeman splitting and circular polarization of positively charged QDs in monolayer WSe₂. a-c, Photoluminescence intensity map versus *B*. Both single peaks (S1 and S2) and doublets (D1 and D2) show Zeeman splitting. Unlike D-peaks, S-peaks show a linear, 'X'-shaped splitting. Colour bars indicate intensity (counts). **d-g**, Splitting energies of S1, D1, S2 and D2 as a function of *B*. D1 and D2 have the same *g*-factor of about 10 and a zero-field splitting energy (δ_0) of about 0.56 meV, consistent with localized, neutral excitons X_d^0 . S1 and S2 display a larger *g*-factor of about 13 and no splitting at zero *B* (dashed lines in **d** and **f** indicate $\delta_0 = 0$ meV). The values of the *g*-factor are shown only as magnitude. **h**, **i**, Degree of circular polarization (DCP), ($I_{\sigma} + I_{\sigma^-}$) of S1 under linear excitation, where I_{σ^+} (or I_{σ^-}) denotes the intensity of the σ^+ (or σ^-) polarized emission. **h**, Colour plot of DCP for S1 in *B*. S1 does not have a circular component at zero *B*, but the magnitude of DCP increases with increasing *B*. **i**, DCP plot for S1 at low *B*. The S1 blue (or red) peak is indicated with a blue (or red) dot. The DCP of the S1 peak at B = 0 is indicated with a yellow square. Sizeable circular components are recovered even at a small *B*. At B = -0.2 T, the DCP of the S1 red (or blue) peak reaches -2.7% (or 31%). The error bars (one standard deviation) are calculated by calibrating the setup by using linearly polarized light and arise from the polarization imperfections. Excitation laser wavelengths are $\lambda = 740$ nm in **a**-c, 750 nm in **d**, **e**, **h** and **i** and 747 nm in **f** and **g**.

conclude that under σ^+ (or σ^-) excitation, we can initialize the spinvalley state of the excess hole to be $|-K,\Uparrow\rangle$ (or $|K,\Downarrow\rangle$). Remarkably, this helicity-based initialization is present even at smallest B as long as the splitting of the two peaks can be resolved (Fig. 4e–h). We quantify the strength of this initialization by calculating the ratio, (I_B+-I_B-) / (I_B++I_B-) , where I_B+ (or I_B-) is the intensity

LETTERS NATURE NANOTECHNOLOGY

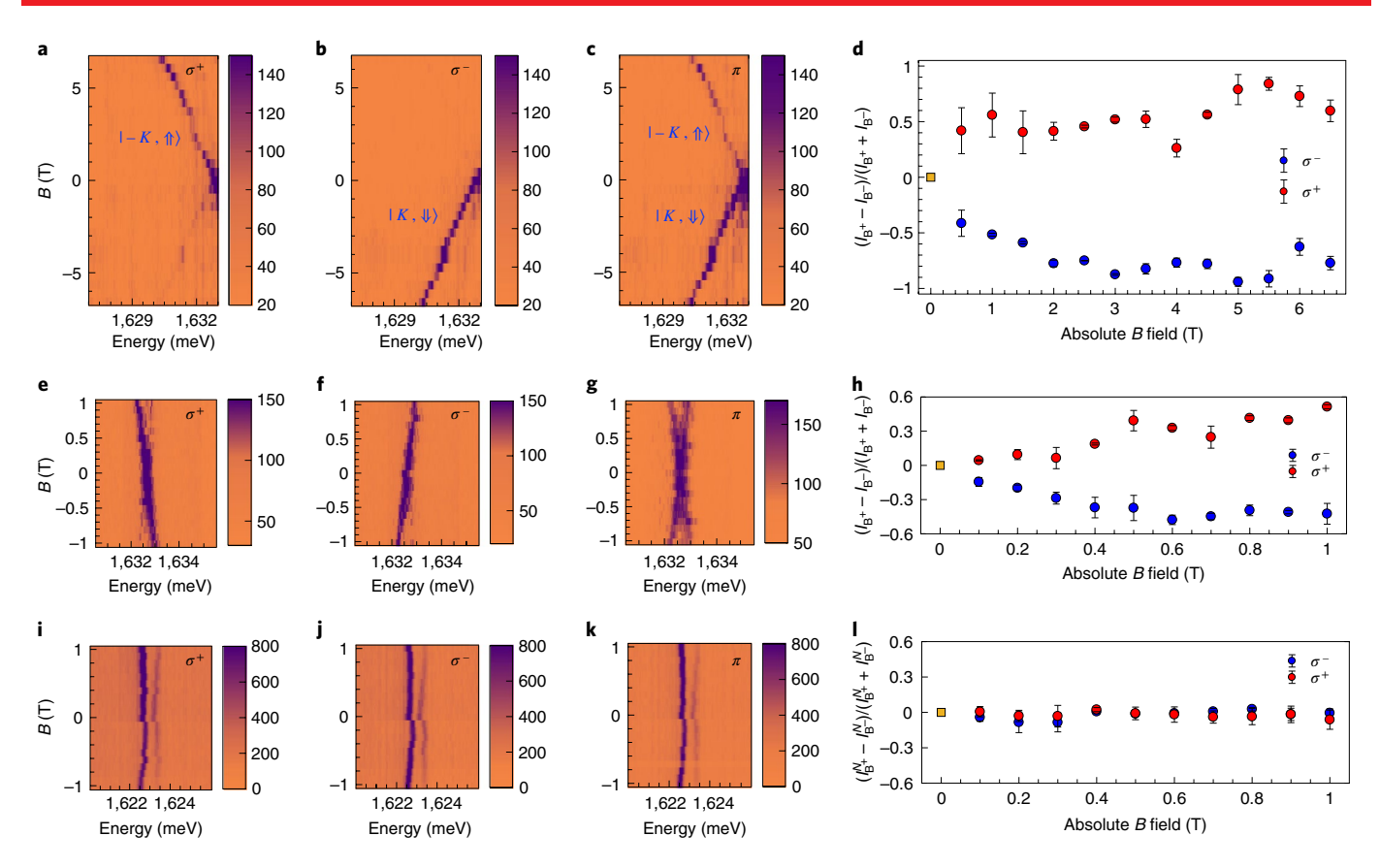


Fig. 4 | Optical initialization of a positively charged QD under magnetic field. a-c, Photoluminescence intensity map of the S2 red peak versus B with σ^+ (**a**), σ^- (**b**) and linear (**c**) excitation. The σ^+ (or σ^-) polarized emission corresponds to recombination of $K_{\rm ex}$ (or $-K_{\rm ex}$) with σ^+ (or σ^-) polarization. $|-K, \Uparrow\rangle$ and $|K, \Downarrow\rangle$ indicate the spin-valley states of the excess hole. The S2 red peak is σ^+ - and σ^- -polarized at positive and negative B, respectively. The S2 red peak is intense when the incident laser is co-polarized with respect to emission, and disappears when it is cross-polarized. Linear excitation (π) does not have selective control of emission preference. **d**, Extracted B-dependent ratio, ($|B_B^+ - B_B^-\rangle$), of the S2 red peak, where $|B_B^+\rangle$ (or $|B_B^-\rangle$) denotes the intensity measured under positive (or negative) B. The ratio approaches unity at high B, implying almost total optical initialization of the spin-valley state. **e-g**, Photoluminescence colour plot of the S2 peak versus B with σ^+ , σ^- and linear excitation at low B. **h**, Extracted ratio ($|B_B^+ - B_B^-\rangle$) of the S2 red peak. **i-k**, Photoluminescence colour plots of D2 doublet with detuning energy similar to that of S2 in **a-h**. No observable selectivity in emission is seen in D2 upon changing the incident polarization. **1**, B-dependent ratio, ($|B_B^+ - B_B^-\rangle$) ($|B_B^+ + B_B^-\rangle$), where $|B_B^+ + B_B^-\rangle$ is the intensity of the D2 red peak normalized by the sum of D2 (red + blue peaks). There is almost no difference between the σ^+ and σ^- excitations, implying that there is no observable optical initialization of the spin-valley state on the neutral exciton. The source of error bars (one standard deviation) is the intensity noise in the data. Laser excitation wavelengths are $\lambda = 747$ nm in **a-h** and 752 nm in **i-l**.

measured under positive (or negative) B (Fig. 4d,f). This ratio of about 50% at 0.5 T approaches unity at higher B, implying initialization with high fidelity (see also Supplementary Figs. 10–13 for the S1-D1 group).

Our observations suggests that at small B, by controlling the helicity of the excitation, we selectively excite K_{ex} or $-K_{ex}$ of X_d^+ , which in turn forces the excess hole to be from the opposite valley, leading to its initialization in a known spin-valley state. As long as the exciton of X_d^+ survives, the spin-valley of the excess hole maintains its state. Even after the recombination of excitons, which takes place after a few nanoseconds^{13,14,16}, one expects the spin-valley of a single, localized hole to be preserved for a much longer time. At zero B and under resonant excitation, the polarization of excitation (linear or circular) should get transferred to the emission owing to the doubly degenerate ground states of X_d^+ . We observe almost zero (or about 20%) circular polarization for S1 (or S2) under circular excitation at zero B (see Supplementary Fig. 5). This behaviour possibly stems from valley relaxation mediated by hyperfine interaction with nuclear spins^{31,32}. To directly measure the spin-valley lifetime after initialization, single-spin Kerr rotation spectroscopy can be used in future studies33.

Although this observation seems very similar to valley polarization of X^0 in TMDs, there is a crucial difference. The reason for valley polarization in photoluminescence of X^0 , even in the presence of electron-hole exchange, is that the photoluminescence lifetime (a few picoseconds) is faster than (or comparable to) the valley mixing time of about 4 ps, assuming an exchange energy of approximately 1 meV23. On the other hand, the photoluminescence lifetime of QDs is of the order of nanoseconds and the helicity-based initialization of the spin-valley stems from the quenching of electron-hole exchange in X_d^+ . To further check this claim, we perform similar measurements on D2 (X_d^0) with similar detuning energy (see Supplementary Figs. 12 and 13). D-peaks are linearly polarized at B = 0 and become circularly polarized at higher B^{13,14,16} (see Supplementary Fig. 9). Figure 4i-l shows that there is almost negligible initialization of the circularly polarized branches of D2 under B, suggesting fast valley relaxation caused by electron-hole exchange.

In conclusion, we have observed positively charged X_d^+ and neutral X_d^0 states of the same QD in a monolayer WSe₂ field effect transistor device. The charged QD hosts an excess hole with a net spin-valley that is opposite to the valley of the electron–hole excitation.

NATURE NANOTECHNOLOGY LETTERS

We find that the electron-hole exchange interaction responsible for valley mixing is quenched in positive, singly charged QDs, which enables optical initialization and read out of its spin-valley under small magnetic fields. Our results show that spin-valley degree is robust in optically active TMD QDs and enables valleytronics on single localized charge carriers.

Online content

Any methods, additional references, Nature Research reporting summaries, source data, statements of data availability and associated accession codes are available at https://doi.org/10.1038/s41565-019-0394-1.

Received: 3 October 2018; Accepted: 28 January 2019; Published online: 4 March 2019

References

- Imamoğlu, A. et al. Quantum information processing using quantum dot spins and cavity-QED. Phys. Rev. Lett. 83, 4204–4207 (1999).
- Giovannetti, V., Lloyd, S. & Maccone, L. Advances in quantum metrology. Nat. Photon. 5, 222–229 (2011).
- Xiao, D., Liu, G.-B., Feng, W., Xu, X. & Yao, W. Coupled spin and valley physics in monolayers of MoS₂ and other group-VI dichalcogenides. *Phys. Rev. Lett.* 108, 196802 (2012).
- 4. Xu, X., Yao, W., Xiao, D. & Heinz, T. F. Spin and pseudospins in layered transition metal dichalcogenides. *Nat. Phys.* **10**, 343–350 (2014).
- Jiang, C. et al. Microsecond dark-exciton valley polarisation memory in two-dimensional heterostructures. *Nat. Commun.* 9, 753 (2018).
- 6. Yang, L. et al. Long-lived nanosecond spin relaxation and spin coherence of electrons in monolayer MoS_2 and WS_2 . Nat. Phys. 11, 830–834 (2015).
- Dey, P. et al. Gate-controlled spin-valley locking of resident carriers in WSe₂ monolayers. *Phys. Rev. Lett.* 119, 137401 (2017).
- Kim, J. et al. Observation of ultralong valley lifetime in WSe₂/MoS₂ heterostructures. Sci. Adv. 3, e1700518 (2017).
- Yan, T., Yang, S., Li, D. & Cui, X. Long valley relaxation time of free carriers in monolayer WSe₂. Phys. Rev. B 95, 241406 (2017).
- Mak, K. F., He, K., Shan, J. & Heinz, T. F. Control of valley polarisation in monolayer MoS₂ by optical helicity. *Nat. Nanotechnol.* 7, 494–498 (2012).
- Zeng, H., Dai, J., Yao, W., Xiao, D. & Cui, X. Valley polarisation in MoS₂ monolayers by optical pumping. *Nat. Nanotechnol.* 7, 490–493 (2012).
- Cao, T. et al. Valley-selective circular dichroism of monolayer molybdenum disulphide. Nat. Commun. 3, 887 (2012).
- 13. Srivastava, A. et al. Optically active quantum dots in monolayer WSe₂. Nat. Nanotechnol. **10**, 491–496 (2015).
- 14. Koperski, M. et al. Single photon emitters in exfoliated WSe₂ structures. *Nat. Nanotechnol.* **10**, 503–506 (2015).
- Chakraborty, C., Kinnischtzke, L., Goodfellow, K. M., Beams, R. & Vamivakas, A. N. Voltage-controlled quantum light from an atomically thin semiconductor. *Nat. Nanotechnol.* 10, 507–511 (2015).
- He, Y.-M. et al. Single quantum emitters in monolayer semiconductors. Nat. Nanotechnol. 10, 497–502 (2015).
- 17. Tonndorf, P. et al. Single-photon emission from localised excitons in an atomically thin semiconductor. *Optica* **2**, 347–352 (2015).
- Branny, A., Kumar, S., Proux, R. & Gerardot, B. D. Deterministic straininduced arrays of quantum emitters in a two-dimensional semiconductor. *Nat. Commun.* 8, 15053 (2017).
- Palacios-Berraquero, C. et al. Large-scale quantum-emitter arrays in atomically thin semiconductors. Nat. Commun. 8, 15093 (2017).
- Schwarz, S. et al. Electrically pumped single-defect light emitters in WSe₂. 2D Mater. 3, 025038 (2016).

- Srivastava, A. et al. Valley Zeeman effect in elementary optical excitations of monolayer WSe₂. Nat. Phys. 11, 141–147 (2015).
- Stier, A. V., McCreary, K. M., Jonker, B. T., Kono, J. & Crooker, S. A. Exciton diamagnetic shifts and valley Zeeman effects in monolayer WS₂ and MoS₂ to 65 tesla. *Nat. Commun.* 7, 10643 (2016).
- Yu, H., Liu, G.-B., Gong, P., Xu, X. & Yao, W. Dirac cones and Dirac saddle points of bright excitons in monolayer transition metal dichalcogenides. *Nat. Commun.* 5, 3876 (2014).
- Courtade, E. et al. Charged excitons in monolayer WSe₂: experiment and theory. Phys. Rev. B 96, 085302 (2017).
- Högele, A. et al. Voltage-controlled optics of a quantum dot. Phys. Rev. Lett. 93, 217401 (2004).
- Chakraborty, C. et al. 3D localised trions in monolayer WSe₂ in a charge tuneable van der Waals heterostructure. Nano Lett. 18, 2859–2863 (2018).
- Regelman, D. V. et al. Optical spectroscopy of single quantum dots at tuneable positive, neutral, and negative charge states. *Phys. Rev. B* 64, 165301 (2001).
- Aivazian, G. et al. Magnetic control of valley pseudospin in monolayer WSe₂. Nat. Phys. 11, 148–152 (2015).
- MacNeill, D. et al. Breaking of valley degeneracy by magnetic field in monolayer MoSe, Phys. Rev. Lett. 114, 037401 (2015).
- 30. Li, Y. et al. Valley splitting and polarisation by the Zeeman effect in monolayer MoSe₂. *Phys. Rev. Lett.* **113**, 266804 (2014).
- Wu, Y., Tong, Q., Liu, G.-B., Yu, H. & Yao, W. Spin-valley qubit in nanostructures of monolayer semiconductors: optical control and hyperfine interaction. *Phys. Rev. B* 93, 045313 (2016).
- Sharma, G., Economou, S. E. & Barnes, E. Interplay of valley polarisation and dynamic nuclear polarisation in 2D transition metal dichalcogenides. *Phys. Rev. B* 96, 125201 (2017).
- Atatüre, M., Dreiser, J., Badolato, A. & Imamoğlu, A. Observation of Faraday rotation from a single confined spin. *Nat. Phys.* 3, 101–106 (2007).

Acknowledgements

We thank A. Imamoğlu and M. Kroner for many discussions. We also acknowledge technical help from T. Neal and E. Liu. A.S. acknowledges support from Emory University startup funds and the NSF through the EFRI programme (grant number EFMA-1741691). Q.X. gratefully acknowledges strong support from Singapore National Research Foundation via an NRF-ANR joint grant (number NRF2017-NRF-ANR002 2D-Chiral) and the Singapore Ministry of Education via an AcRF Tier2 grant (number MOE2017-T2-1-040) and Tier1 grants (RG 113/16 and RG 194/17).

Author contributions

X.L. and A.S. conceived and designed the experiments. X.L., X.C., S.D., Q.Y. and W.L. performed the experiments. X.L. and X.W. prepared the samples. X.L., X.C., S.D., Q.X. and A.S. analysed the data. Q.X. contributed materials. X.L. and A.S. co-wrote the paper.

Competing interests

The authors declare no competing interests.

Additional information

Supplementary information is available for this paper at https://doi.org/10.1038/s41565-019-0394-1.

Reprints and permissions information is available at www.nature.com/reprints.

Correspondence and requests for materials should be addressed to X.L. or A.S.

Journal peer review information: *Nature Nanotechnology* thanks Ziliang Ye and other anonymous reviewer(s) for their contribution to the peer review of this work.

Publisher's note: Springer Nature remains neutral with regard to jurisdictional claims in published maps and institutional affiliations.

© The Author(s), under exclusive licence to Springer Nature Limited 2019

LETTERS NATURE NANOTECHNOLOGY

Methods

Sample fabrication. We used the polydimethylsiloxane-based dry transfer method to fabricate a WSe₂/BN (crystals from HQ graphene) stack on a degenerately doped Si (Si*+) substrate with 285 nm SiO₂ on top. Electron beam lithography was used to deposit 30-nm Pd/80-nm Au metal contacts on WSe₂, which act as source and drain electrodes. The charge carrier density in WSe₂ was controlled by applying voltage (with a Keithley 2400 sourcemeter) to the Si*+ substrate, with the 285-nm SiO₂ acting as the gate dielectric.

Photoluminescence spectroscopy. The sample was loaded into a closed-cycle cryostat (BlueFors cryogenics) with magnetic field ranging from $-8\,\mathrm{T}$ to $+8\,\mathrm{T}$ and cooled down to about 3.5 K. A piezo controller (Attocube systems) was used to position the sample. Photoluminescence spectroscopy was performed using a home-built confocal microscope set-up. The emission was collected using an aspheric lens (numerical aperture 0.55) and directed to a high-resolution (focal length 750 mm) spectrometer where it was dispersed by a 1,200 g mm^-1 grating (blazed at 750 nm). A liquid nitrogen-cooled charge coupled device (Princeton Instruments SP-2750, PyLoN 1,340×400 pixels CCD) was used as detector. We used a mode-hop-free tuneable continuous-wave Tissapphire laser (M Squared Lasers) with resolution of 0.1 pm and power of 300 nW or 400 nW

(except during power dependence measurements) as the excitation source. The spot size for the Ti:sapphire laser was about 1 µm. Photoluminescence excitation spectroscopy was performed below the free exciton energy in order to identify resonances for a given QD to increase its emission intensity. Polarization of the incident laser was controlled by using a polarizer together with a fullwave liquid crystal retarder. Circular-polarization-resolved measurements were performed with a $\lambda/4$ (achromatic, 690–1,200 nm) plate placed before the Wollaston prism. One can collect σ^+ and σ^- components of the polarization simultaneously. The influence of blinking on polarization measurements is eliminated in this setup. Circular emission from QD was converted into linearly polarized light after passing through the $\lambda/4$ plate. The Wollaston prism separates light into s- and p-components. Another $\lambda/4$ plate (zero order at 780 nm) is placed after the Wollaston prism to convert the linearly polarized light into a circularly polarized signal, so that the signal will be insensitive to the grating efficiency. In all the magnetic field dependence measurements, *B* is applied perpendicular to the plane of the sample.

Data availability

The data that support the plots within this paper and other findings of this study are available from the corresponding author upon reasonable request.